Nanoscale Research Letters
a SpringerOpen Journal

NANO EXPRESS Open Access

Structural and optical characterization of pure Si-rich nitride thin films

Olivier Debieu[1*], Ramesh Pratibha Nalini[1], Julien Cardin[1], Xavier Portier[1], Jacques Perrière[2] and Fabrice Gourbilleau[1]

Abstract

The specific dependence of the Si content on the structural and optical properties of O- and H-free Si-rich nitride ($SiN_{x>1.33}$) thin films deposited by magnetron sputtering is investigated. A semiempirical relation between the composition and the refractive index was found. In the absence of Si-H, N-H, and Si-O vibration modes in the FTIR spectra, the transverse and longitudinal optical (TO-LO) Si-N stretching pair modes could be unambiguously identified using the Berreman effect. With increasing Si content, the LO and the TO bands shifted to lower wavenumbers, and the LO band intensity dropped suggesting that the films became more disordered. Besides, the LO and the TO bands shifted to higher wavenumbers with increasing annealing temperature which may result from the phase separation between Si nanoparticles (Si-np) and the host medium. Indeed, XRD and Raman measurements showed that crystalline Si-np formed upon 1100°C annealing but only for $SiN_{x<0.8}$. Besides, quantum confinement effects on the Raman peaks of crystalline Si-np, which were observed by HRTEM, were evidenced for Si-np average sizes between 3 and 6 nm. *A contrario*, visible photoluminescence (PL) was only observed for $SiN_{x>0.9}$, demonstrating that this PL is not originating from confined states in crystalline Si-np. As an additional proof, the PL was quenched while crystalline Si-np could be formed by laser annealing. Besides, the PL cannot be explained neither by defect states in the bandgap nor by tail to tail recombination. The PL properties of $SiN_{x>0.9}$ could be then due to a size effect of Si-np but having an amorphous phase.

Keywords: Silicon nitride, Silicon nanocrystals, Amorphous silicon nanoparticles, FTIR, Raman, XRD, Laser annealing, Photoluminescence

Background

Since the discovery of efficient visible photoluminescence (PL) of silicon nanoparticles (Si-np) due to quantum confinement effects (QCE) [1], the possibility of bandgap engineering of Si-based materials through the Si-np size control makes Si-based nanostructured material attracting for future applications in optoelectronics as low-cost, miniaturized, and CMOS-compatible, light-emitting devices (LEDs), laser, as well as photovoltaic devices. In the past, researches were focused on luminescent Si-np embedded in Si oxide media. However, the insulating nature of Si oxide remains a barrier for the production of future electrically pumped LEDs and efficient photovoltaic cells. This detrimental aspect can be overcomed to an extent, using a higher conductive host medium like Si nitride which has a lower bandgap energy than SiO_2.

The first results on Si nitride are promising since many researchers have reported on efficient visible PL with tunable light emission via the change of the Si nitride composition. However, it also turns out that N-rich nitride [2-4] and Si-rich nitride thin films containing amorphous [5-8] or crystalline [9-14] Si-np or without Si-np [15-18] can exhibit PL in the same spectral range. As a result, the mechanism of the PL in Si nitride is still a controversial subject in the literature. QCE in amorphous or crystalline Si-np, defect states in the bandgap, and band tail recombination have been proposed to account for the PL. However, since the synthesis methods were mostly based on chemical vapor deposition techniques, most of the films contained a significant amount of hydrogen [2,5,8,10,11,13,14,16] and, in some cases, of oxygen [19,20], which can both contribute to the PL.

* Correspondence: o_debieu@yahoo.fr
[1]CIMAP, UMR 6252 CNRS-ENSICAEN-CEA-UCBN, Ensicaen, 6 Bd Maréchal Juin, 14050 Caen, cedex 4, France
Full list of author information is available at the end of the article

Springer

© 2013 Debieu et al.; licensee Springer. This is an Open Access article distributed under the terms of the Creative Commons Attribution License (http://creativecommons.org/licenses/by/2.0), which permits unrestricted use, distribution, and reproduction in any medium, provided the original work is properly cited.

Consequently, it is difficult to experimentally distinguish the mechanisms of the PL.

Then, this article is significant since we report on the structural and optical properties of Si-rich $SiN_{x<1.33}$ thin films devoid of hydrogen and oxygen. The films were deposited by radio frequency (RF) magnetron sputtering. The excess of Si incorporated during the sputtering process makes possible the formation of Si-np during a suitable annealing. The microstructural properties of the films with regard to the composition and the annealing temperature are investigated. The possible contributions of the Si nitride medium and of Si-np formed during thermal annealing, or laser annealing, on the origin of the PL are discussed notably as a function of the Si-np phase (crystalline or amorphous).

Methods

In this work, pure amorphous Si-rich SiN_x thin films were deposited on p-type 250-μm-thick (100) Si wafers and on fused silica substrates by two methods of RF magnetron sputtering using argon as the main sputtering gas. The films were deposited either by N_2-reactive sputtering of a Si target or by co-sputtering of Si_3N_4 and Si targets. The Si content was monitored either by the N_2/Ar partial pressure ratio ($\equiv Ar/N_2$) or by the RF target power ratio $P_{Si}/(P_{Si} + P_{Si3N4}) \equiv Si/Si_3N_4$. The grown temperatures were 200°C and 500°C, and the plasma pressures were 2 and 3 mTorr. We adjusted the deposition time to ensure that the films thicknesses were of the same order of magnitude (100 to 200 nm) in order to avoid any effect on the optical and structural properties. The films were subsequently annealed in a N_2 gas flow in a tubular furnace during 1 h.

The layer compositions were determined by Rutherford backscattering spectrometry (RBS). RBS measurements were carried out at room temperature using a 1.9 MeV $^4He^+$ ion beam with an incident direction normal to the sample surface. The backscattered ions were collected at a scattering angle of 165°. The analysis of the RBS spectra, which were performed using the simulation code SIMNRA [21], enables us to quantify (a) the atomic fraction of the various elements with an accuracy of 0.8 at.% for Si and N and 0.2 at.% for Ar and (b) to determine the atomic areal densities of the films. The infrared absorption properties were investigated by means of a Thermo Nicolet (Nexus model 670) Fourier transform infrared (FTIR) spectrometer. The band positions were obtained by fitting the data with Gaussians. The film microstructure was investigated by Raman spectroscopy with a 532-nm continuous-wave laser illumination with a spot diameter of 0.8 μm. Several neutral density filters were employed to tune the excitation power density from 0.14 to 1.4 MW/cm^2. A dispersive Horiba Jobin-Yvon Raman spectrometer with a resolution of 1.57 cm^{-1}, equipped with a confocal microprobe and a CCD camera, was used to acquire the Stokes scattering spectra of the thin layers that were exclusively deposited on fused silica substrates. We also studied the film microstructure by X-ray diffraction (XRD) using a Phillips X'PERT HPD Pro device with Cu K_λ radiation (λ = 0.1514 nm) at a fixed grazing incidence angle of 0.5°. Asymmetric grazing geometry was chosen to increase the material volume interacting with the X-ray beam and to eliminate the contribution of the Si substrate. Moreover, the structure was investigated by high-resolution transmission electron microscopy (HRTEM) on cross-sectional samples using a JEOL 2010F (200 kV) microscope.

The optical properties of the films were investigated by spectroscopic ellipsometry using a Jobin-Yvon ellipsometer (UVISEL) with an incident angle of 66.2°. The experimental data were fitted by a dispersion law based on the Forouhi-Bloomer model for amorphous semiconducting and insulating materials [22] using the DeltaPsi2 software [23] which determines the refractive index n, the absorption coefficient α versus the photon energy, and the layer thicknesses. The PL spectra were measured using the 457-nm lines of an Ar^+ ion laser (12.7 W/cm^2) and a fast Hamamatsu photomultiplier after dispersion of the light in a Jobin-Yvon TRIAX-180 monochromator. The PL measurements were corrected from the spectral response of the PL setup.

Results

We first report on the combined analysis of the SiN_x film composition by RBS and ellipsometry. Then, the microstructure and the optical properties of the films are investigated as a function of the composition, as well as the annealing temperature.

RBS

Figure 1 shows a typical RBS spectrum of a SiN_x layer with the corresponding simulation curve obtained using the SIMNRA code with a composition of 49.8, 48.6, and 1.6 at.% of Si, N, and Ar, respectively. The presence of residual Ar attests that the film is as-deposited. Interestingly, no oxygen was detected in all RBS spectra whatever the synthesis method, suggesting that the films do not contain oxygen or less than the detection threshold (0.2 at.%).

Ellipsometry

Figure 2 shows the evolution of the dispersion curves of SiN_x films deposited on Si wafer by the co-sputtering and N_2-reactive methods with the synthesis parameters Si/Si_3N_4 and N_2/Ar, respectively. The dispersion curves progressively change from the one of stoichiometric amorphous Si nitride (a-Si_3N_4) to that of amorphous Si (a-Si) with increasing Si/Si_3N_4 or decreasing N_2/Ar. This evolution is due to the only increase of the Si incorporation

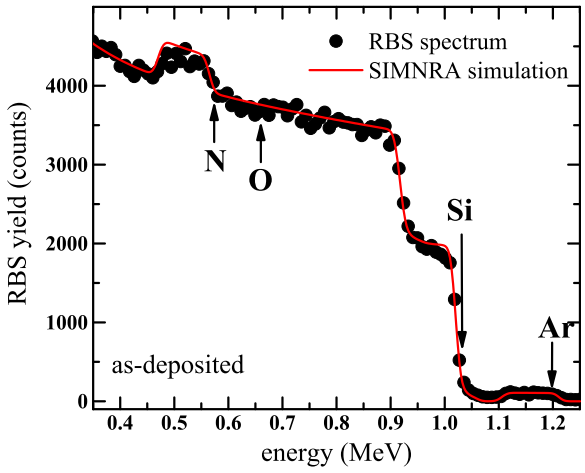

Figure 1 RBS spectrum of a SiN_x layer with the corresponding SIMNRA simulation curve. The film was deposited on a Si substrate by the N_2-reactive method. Surface peaks of N, O, Si, and Ar are indicated by arrows.

during the growth, which is explained by the drop of the amount of reaction between N_2 and Si for the N_2-reactive method, and by the increase of the Si content into the plasma for the co-sputtering method. Indeed, one can notice that the dispersion curves change in the same way independently of the deposition method.

Figure 3 shows the evolution of the refractive index of SiN_x films (given at 1.95 eV) produced by the two methods as a function of the [N]/[Si] ratio x. The numerous results

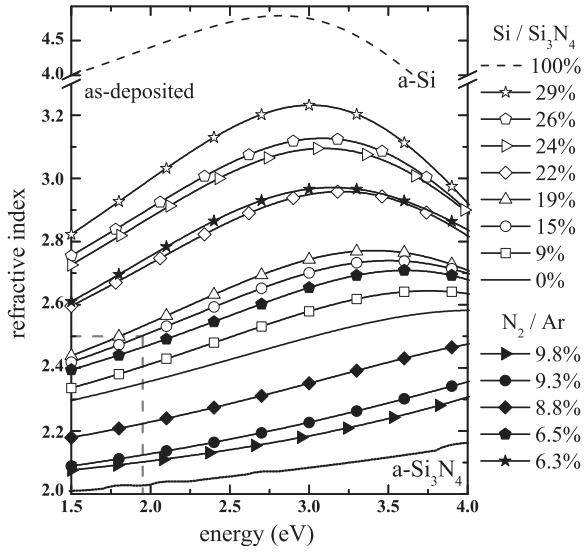

Figure 2 Evolution of the dispersion curves of SiN_x thin films. The films were produced by the N_2-reactive (full symbols) and the co-sputtering (empty symbols) methods as a function of the Ar/N_2 gas flow ratio and the Si/Si_3N_4 target power ratio, respectively. The dispersion curve of Si_3N_4 from [28] is shown for comparison.

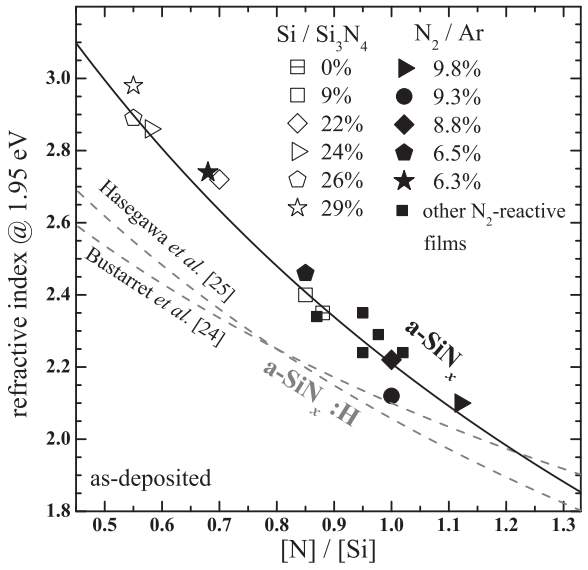

Figure 3 Evolution of the refractive index of SiN_x thin films. The films were produced by the N_2-reactive and the co-sputtering methods as a function of [N]/[Si] ratio. The data are compared with a new model (black curve) and with two models (dashed curves) but concerning hydrogenated films.

show that x progressively increases independently of the synthesis method with increasing either Ar/N_2 or Si/Si_3N_4. Bustarret et al. [24] proposed that the refractive index n could be represented as the bonding-density-weighted linear combination of reference refractive indexes taken at $x = 0$ and $x = 4/3$ using the empirical relation:

$$x = 4/3(n_{a-si} - n)/(n + n_{a-Si} - 2n_{a-Si_3N_4}) \quad (1)$$

Nevertheless, one can notice in Figure 3 that our experimental results progressively diverge from the models obtained by this group and also by Hasegawa et al. [25] while x is decreased. However, the two groups both studied hydrogenated SiN_x films (SiN_x:H) in contrast to our results. Besides, these latter authors have shown that the Si-H density increased while x was experimentally decreased. Consequently, the drop of n is explained by the H incorporation in their material as suggested elsewhere [26]. However, we could use this model to fit the experimental data but using the refractive index of a-Si ($n_{a\text{-Si}} = 4.37$, see Figure 2) instead of hydrogenated a-Si ($n_{a\text{-Si:H}} = 3.3$) used by Bustarret et al. [24]. This shows again the influence of H on the optical properties of the films. We obtained $n_{a\text{-}Si_3N_4} = 1.85$, which is similar to many previous results [25-27], but is lower than 2.03 that is commonly used for a-Si_3N_4 [28]. This difference could be explained by the incorporation of voids in the microstructure [27] as attested by the presence of residual Ar atoms detected by RBS in the as-deposited films. Besides, this explanation is confirmed by the

density ρ_v of our SiN_x films which was calculated using the atomic areal density ρ_s, and the film thickness d, obtained by RBS and ellipsometry analyses, respectively, with the following relation: $\rho_v = \rho_s / d$. We found that the density varied from 2.4 to 2.8 g/cm^3, which is again sensibly lower than that of a-Si_3N_4 of 3.1 g/cm^3 reported in the literature [29].

Considering the RBS and the ellipsometry spectra, we have produced thin SiN_x films with various compositions that do not depend on the synthesis method, but only on the Si content. As a consequence, n is a precise indicator of the composition that will be used in the following sections.

FTIR

Figure 4 shows the typical FTIR spectra of a SiN_x film with a low refractive index of 2.1 ($SiN_{1.12}$) which were recorded with a normal incidence and with an incidence angle of 65°. One can observe only one absorption band centered at 833 cm^{-1} in the spectrum measured with the normal incidence, whereas an additional shoulder at 1115 cm^{-1} emerged while the incidence angle was changed to 65°. Moreover, it is essential to note that no other absorption bands were discernible in the 700 to 4000 cm^{-1} spectral range whatever the deposition approach. No Si-O absorption bands (transverse optical (TO_4) at 1200 cm^{-1}, longitudinal optical (LO_4) at 1160 cm^{-1}, TO_3 at 1020 to 1,090 cm^{-1}, LO_3 at 1215 to 1260 cm^{-1}, TO_2 at 810 cm^{-1}, and LO_2 at 820 cm^{-1}) [30,31] were detected in all spectra. This demonstrates the absence of O contamination that has been also confirmed by RBS and the absence of any oxide layers at the interface between the Si-wafer and the SiN_x layers which has been confirmed by HRTEM observations. Besides, no absorption bands of Si-H stretching mode in the 2090 to 2200 cm^{-1} spectral domain were detected because of our synthesis methods involving no hydrogen. Since the latter band is generally the most intense Si-H vibration mode observed in SiN_x:H, one can then conclude on the absence of the Si-H wagging (630 to 650 cm^{-1}) and asymmetric stretching (840 to 900 cm^{-1}) modes in the spectra [24,25,27,32-34]. In the same manner, no absorption bands of N-H stretching mode were detected in the 3320 to 2500 cm^{-1} spectral region suggesting that the N-H bending (1140 to 1200 cm^{-1}) modes are also absent in our spectra [24,25,32,33]. As a consequence, the 833-cm^{-1} band and the 1115-cm^{-1} shoulder can be unambiguously assigned to the transverse (TO) and the longitudinal (LO) modes of the asymmetric Si-N stretching vibration, respectively [24,33-37]. The TO-LO splitting is due to the Berreman effect [38] according to which only the TO mode is IR active in normal incidence, and the shoulder observed with an incidence angle of 65° corresponds to the LO mode. Then, the analysis of the FTIR spectra in the 700 to 1200 spectral domain is particularly interesting since it definitely concerns the Si-N bonding alone, in contrast to many works on the FTIR study of SiN_x:H films [5,27,32-34,39], Si nitride layers containing oxygen [19,20], or SiN_x layers stacked between Si oxide layers [17,40].

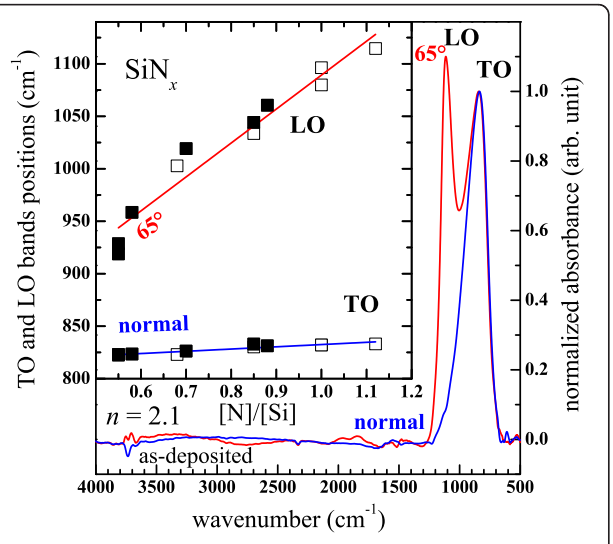

Figure 4 FTIR spectra of a SiN_x thin film. The films were deposited by the N_2-reactive method recorded with a normal incidence and with an incidence angle of 65°. The inset shows the TO and LO band positions of SiN_x layers deposited by the N_2-reactive (full squares) and the co-sputtering (empty squares) methods as a function of the composition.

Figure 5 shows the evolution of the FTIR spectra of SiN_x thin films measured with the two incidence angles. The spectra are arranged with increasing order of n of SiN_x films deposited by both methods. One can notice that the evolution of the FTIR spectra is not influenced by the deposition method but only by the composition. The spectra in Figure 5a showing the TO band only change slightly with n, whereas the evolution of the spectra in Figure 5b is more pronounced because of the significant blueshift of the LO band and the concomitant increase of its intensity with decreasing n. The TO band shifts to higher wavenumbers as well but with a lesser extent.

Similar blueshifts of the TO band [5,25,27,32-34] and of the LO band [24,27,33] were also observed in SiN_x:H films. Lucovsky et al. [32] explained the TO band blueshift by the incorporation of H. They suggested that one of the near silicon atoms of the N(–Si)$_3$ bonding configuration where Si has only one N neighbor is replaced by a H atom. The H incorporation was also evoked to be responsible for the LO band blueshift in SiN_x:H [24,27,33,39]. However, our spectra in Figure 5 demonstrate that these two blueshifts are not necessarily linked to H. Besides, similar blueshifts of the TO band [15,35] and of the LO band [35]

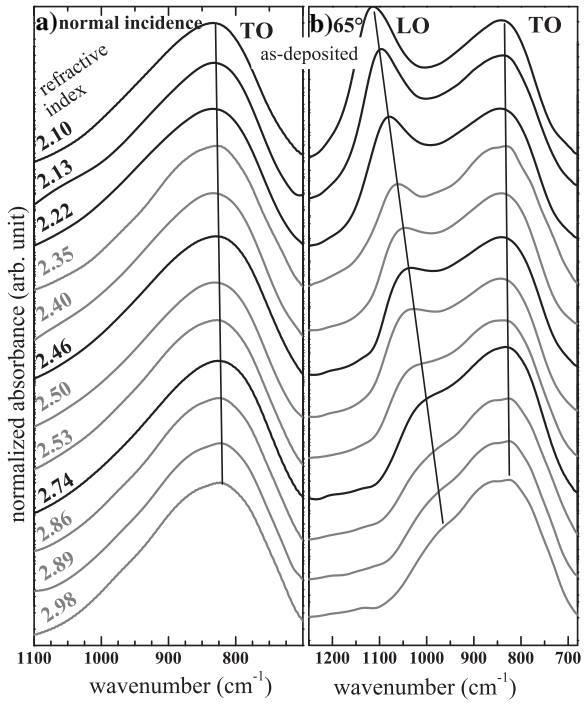

Figure 5 Evolution of the FTIR spectra of SiN_x with the refractive index. The FTIR spectra of the layers deposited by the N_2-reactive (black) and the co-sputtering (gray) methods were measured with a normal incidence (**a**) and with an incidence angle of 65° (**b**).

have also been reported in O- and H-free SiN_x thin films while the Si content was decreased. As a consequence, these two blueshifts are partly or completely due to some change of the [N]/[Si] ratio in the case of SiN_x:H or pure SiN_x, respectively. The change in the positions of the TO and the LO modes of Si-N absorption bands are due to some modifications intrinsic to the Si-N binding configuration. In their calculation, Hasegawa et al. [25] have predicted that the blueshift of the TO mode is linked to the decrease of the Si-N bond length which is caused by a compositional change of SiN_x [25,41]. In addition to this, some stress in the films induced by the Si incorporation may also contribute to such shifts [35]. Moreover, one can assume that the TO-LO coupling of the Si-N asymmetric stretching modes is induced by the disorder in the material in the same manner as that established in Si oxide [42,43]. Consequently, the increase of the LO band intensity is a signature of the ordering of the films while the Si content is decreased.

The inset of Figure 4 shows the TO and LO band positions as a function of the stoichiometry. Again, one can notice that the LO band position is more sensitive to the composition than that of the TO band. The LO mode position is obviously a better indicator of the composition of Si-rich SiN_x than that of the TO band, as mentioned elsewhere [35]. We found that the TO and the LO band positions increase linearly with increasing Si/N ratio x following the two relations:

$$\nu_{\mathrm{TO}}(x) = 21.4(x - 4/3) + \nu_{\mathrm{TO}}(4/3) \quad (2)$$

$$\nu_{\mathrm{LO}}(x) = 323.4(x - 4/3) + \nu_{\mathrm{LO}}(4/3) \quad (3)$$

where $\nu_{\mathrm{TO}}(x)$ and $\nu_{\mathrm{LO}}(x)$ are the TO and the LO band positions, respectively, and $\nu_{\mathrm{TO}}(4/3)$ and $\nu_{\mathrm{LO}}(4/3)$ are the TO and the LO band positions calculated for $x = 4/3$, which correspond to the stoichiometric condition, respectively. We found $\nu_{\mathrm{TO}}(4/3) = 840\ \mathrm{cm}^{-1}$ which is interestingly the value attributed to the Si-N stretching vibration of an isolated nitrogen in a N-Si_3 network [33,44] and $\nu_{\mathrm{LO}}(4/3) = 1197\ \mathrm{cm}^{-1}$. These relations can be used to estimate the composition of as-deposited Si-rich SiN_x films in the same way as the empirical one concerning Si-rich silicon oxide [30].

In Figure 6a, the effect of the annealing on the FTIR spectra of a SiN_x film with $n = 2.22$ is shown. It is seen that the intensity of the TO mode increases with increasing annealing temperature which is manifestly due to the increase in the amount of Si-N bonds. It is also seen that the TO peak position slightly shifts to higher wavenumbers. Moreover, Figure 6b shows that the LO band evolves similarly, *i.e.*, an increase of its intensity and a significant blueshift. All these observations indicate a rearrangement of the Si nitride network toward that of the stoichiometric structure with a lower structural disorder. This can be due to a phase separation between Si and Si nitride.

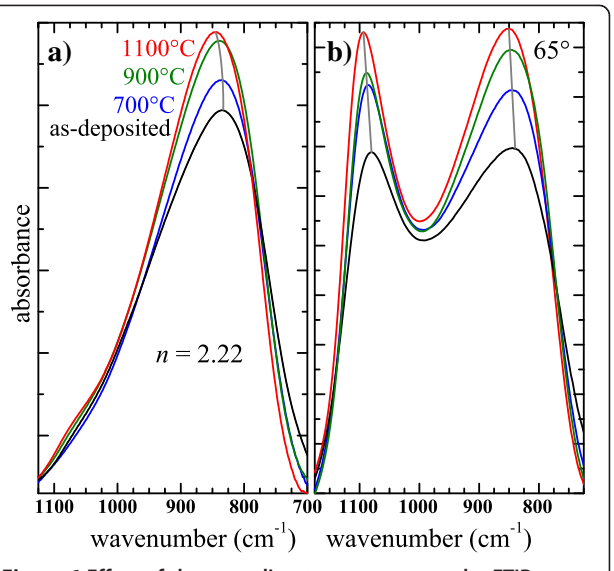

Figure 6 Effect of the annealing temperature on the FTIR spectra of SiN_x. The FTIR spectra were recorded under normal incidence (**a**) and with an angle of 65° (**b**).

Raman spectroscopy

Figure 7 shows the evolution of the Raman spectra of SiN_x thin layers deposited on fused silica with various Si contents and with various annealing temperatures. Again, it is seen that the evolution of the Raman spectra does not depend on the deposition methods but only on the composition that is set by *n*. Upon annealing at 900°C, the two broad vibration bands of the transverse acoustic (TA) phonon and of the TO phonon of a-Si at 150 and 480 cm^{-1}, respectively, became clearly narrower and more pronounced (Figure 7). This evolution can be explained by the formation of small amorphous Si-np [45]. Unlike this deduction, the appearance of new sharp peaks slightly shifted towards lower wavenumbers compared to bulk crystalline Si (c-Si) at approximately 520 cm^{-1} upon annealing at 1100°C as shown in Figure 7b, which unequivocally demonstrates the formation of small crystalline Si-np. Besides, the formation of a c-Si phase is also consistent with the appearance of a weak peak at 300 cm^{-1} that is attributed to the second order of the transverse acoustic (2TA) phonon mode in the thin films containing a high Si content (n = 2.89 and 2.98). It is seen that the condensation of the excess of Si in small crystalline Si-np during the annealing at 1100°C occurs but only in thin films having a refractive index higher than 2.5 (Figure 7b) or maybe equal to 2.5 as indicated by the presence of a weak shoulder (see the arrow) in Figure 7a. Nevertheless, thin films with a low Si content ($SiN_{x\ >\ 0.8}$, see Figure 3) could also contain small Si-np upon annealing at 1100°C but having an amorphous structure.

Figure 8 shows the Raman spectra of the thin films with n > 2.5 (Figure 7b) after annealing at 1100°C. A low excitation energy density of 0.14 MW/cm^2 was used to record these spectra in order to avoid any heating and induced stress of the films that may affect the Raman spectra of crystalline Si-np [46]. One can observe that the c-Si peaks progressively shift to higher wavenumbers toward the peak position of bulk c-Si with increasing *n*. This progressive shift is related to a QCE on the optical phonon in confined crystalline Si-np [46-49], as it is seen in the inset of Figure 8 where the Raman shift is plotted as a function of the diameter. The Raman shift was obtained by fitting the Raman signal with the asymmetric Lorentzian functions, and the particle size corresponded to the maximum of the lognormal distribution of crystalline Si-np sizes measured by HRTEM (see Figure 9). Then, we compared our experimental results with the Richter, Wang, and Ley (RWL) model [47] and the bond polarizability (BP) model [48] that account for the QCE on

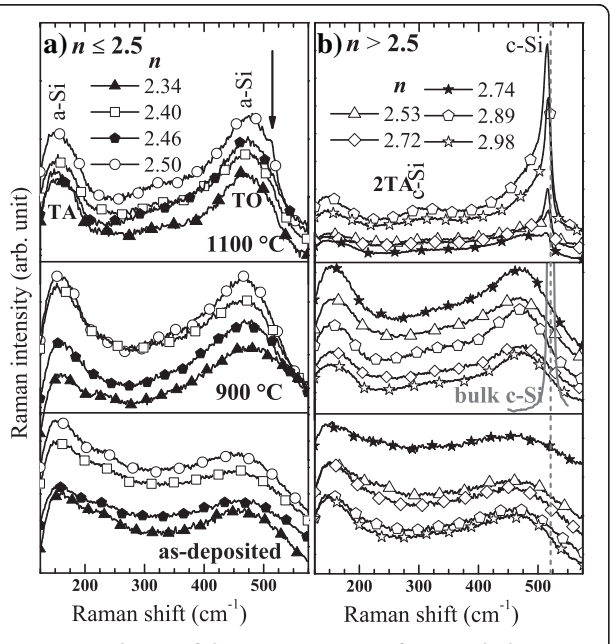

Figure 7 Evolution of the Raman spectra of SiN_x with the refractive index and the annealing temperature. Effect of the annealing temperature on the Raman spectra of SiN_x thin layers deposited on fused silica with a refractive index below 2.5 (**a**) and above (**b**). It independently concerns films produced by the N_2-reactive (full symbols) and the co-sputtering (empty symbols) methods. The excitation power density was 0.46 MW/cm^2.

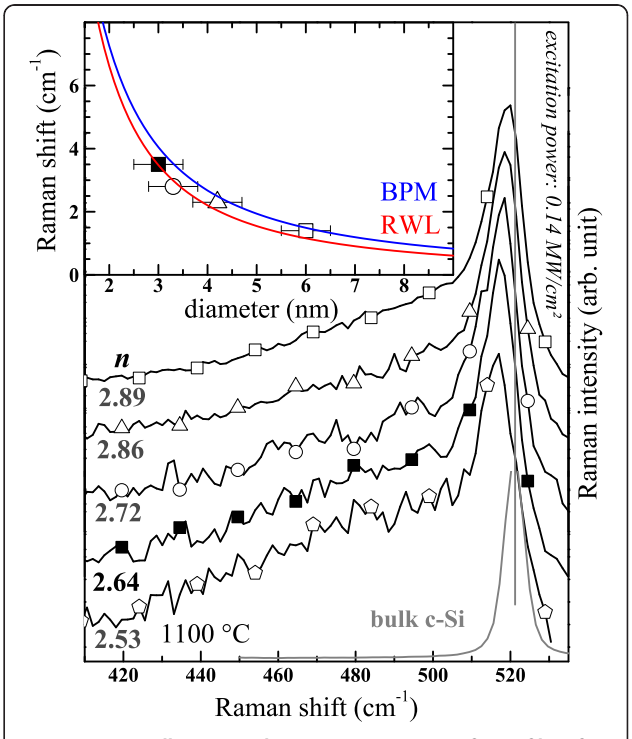

Figure 8 Crystalline Si peaks in Raman spectra of SiN_x films for various refractive indexes. Raman spectra of the films produced by the N_2-reactive and the co-sputtering methods are displayed with empty and full symbols, respectively. The inset shows the Raman frequency redshift as a function of the crystalline Si-np average size measured by HRTEM. The curves of the RWL and BP models are shown for comparison.

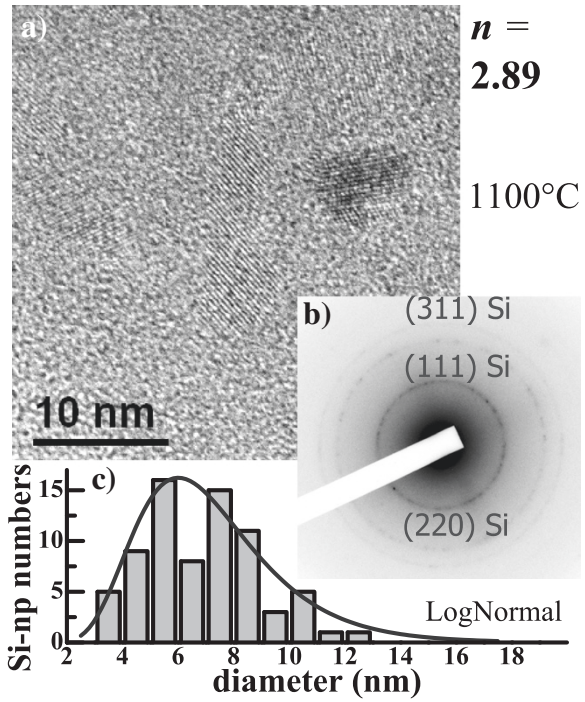

Figure 9 HRTEM image (a), diffraction pattern (b), and Si nanocrystal size distribution (c).

optical phonons in crystalline Si-np. In these two models, the Raman redshift can be presented as a function of the Si-np size using the analytical expression:

$$\Delta\omega = \beta(a/d)^{\gamma} \quad (4)$$

where $\Delta\omega$ is the frequency redshift; a, the Si lattice parameter (a = 0.543 nm); d, the crystalline Si-np diameter; and β and γ, the model parameters (β = 52.3 cm^{-1} and γ = 1.586 for the RWL model, and β = 47.41 cm^{-1} and γ = 1.44 for the BP model). Interestingly, one can notice that our experimental results are in good agreement with the previous works suggesting that the latter models can be applied to crystalline Si-np embedded in Si nitride as well.

HRTEM

In order to further investigate the microstructure of the 1100°C-annealed films, HRTEM observations have been performed on several thin films with various n > 2.5. Figure 9b shows the diffraction pattern of one film with n = 2.89. One can observe three quasi-continuous rings corresponding to various orientations of c-Si because of the presence of randomly oriented crystalline Si-np. These numerous crystalline Si-np can be easily distinguished from the host matrix (Figure 9a) because of the lattice fringes of c-Si. They are rather small with an average size of about 6.0 ± 0.5 nm (Figure 9c).

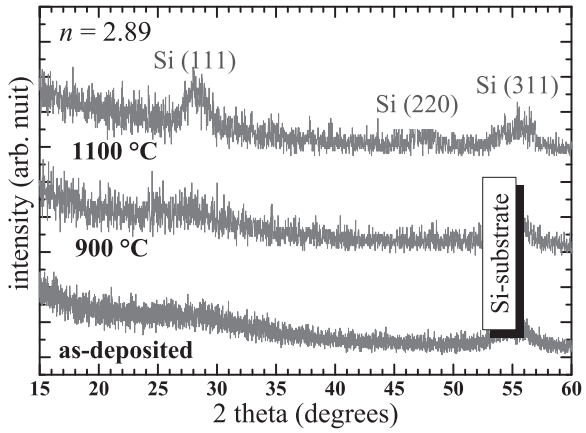

Figure 10 Evolution of the XRD pattern of a SiN_x layer as a function of the annealing temperature.

XRD

Figure 10 shows the effect of the annealing temperature on the XRD patterns of one SiN_x layer produced by the co-sputtering method with n = 2.89. One can observe that two new peaks of c-Si with the (111) and (220) orientations distinctly emerge in the XRD pattern upon annealing at 1100°C, which demonstrates the formation of a c-Si phase in the material.

In Figure 11, the evolution of the XRD pattern of the 1100°C-annealed films with n is shown. Again, we could

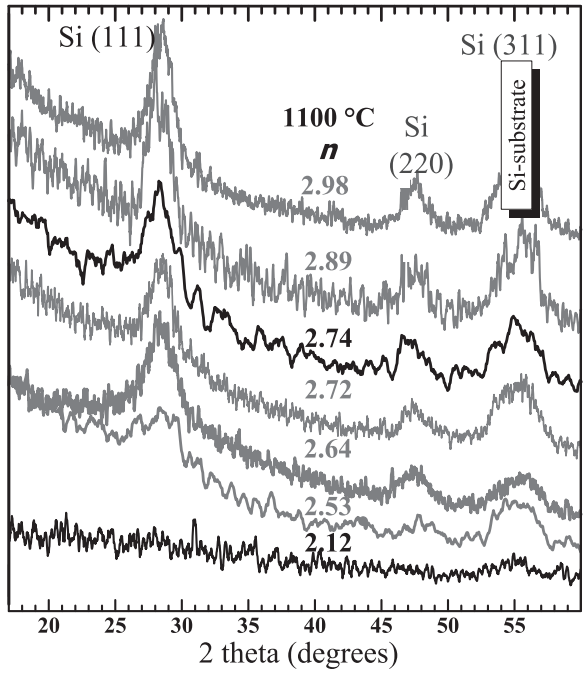

Figure 11 Evolution of XRD pattern of 1100°C-annealed SiN_x layers with the refractive index. XRD curves of thin films produced by the N_2-reactive and the co-sputtering methods are displayed in black and gray, respectively.

not notice any dependence of the synthesis method on the structure since the spectra of the two films produced by the co-sputtering and the N_2-reactive methods which have a close refractive index of 2.72 and 2.74, respectively, are very similar. The XRD patterns depend only on the Si content given by *n*. One can notice that the thin films with $n = 2.12$ do not show any c-Si peak with the exception of the (311) c-Si peak emanating from the substrate. This is in contrast with the spectra of thin films with a higher refractive index ($n > 2.5$) that also show the (111) and (220) c-Si diffraction peaks attesting the presence of crystalline Si-np. Besides, the XRD results are in perfect agreement with the Raman spectra shown in Figure 7, since the c-Si Raman peaks were also detected but only when *n* was above 2.5 ($SiN_{x<0.8}$).

Photoluminescence

Figure 12 shows the PL and the absorption spectra of several SiN_x thin films with various *n*. In the right part of the figure, it is seen that the absorption rises with increasing *n* which is explained by the increase of the Si content. In the same time, we observed a progressive redshift of the PL bands with a concomitant increase of their widths as displayed in the inset. Moreover, one can notice that the PL intensity significantly increases while *n* increases from 2.01 to 2.12, which is partly explained by the rise of the absorption. Reminding that FTIR spectra showed that the disorder increased with increasing *n*, the increase of the non-radiative recombination rate would then explain the decrease of the PL intensity while *n* reaches 2.14. Besides, thin films with $n > 2.4$ ($SiN_{x<0.85}$) did not exhibit any PL even after annealing with various temperatures ranging up to 1100°C. The typical variation of the PL intensity of one luminescent film with the annealing temperature is shown in Figure 13. Interestingly, as-deposited films showed no PL, and it is seen that the highest integrated PL intensity was found at 900°C. The origin of the visible PL easily perceivable by the naked eye is investigated in the 'Discussion'.

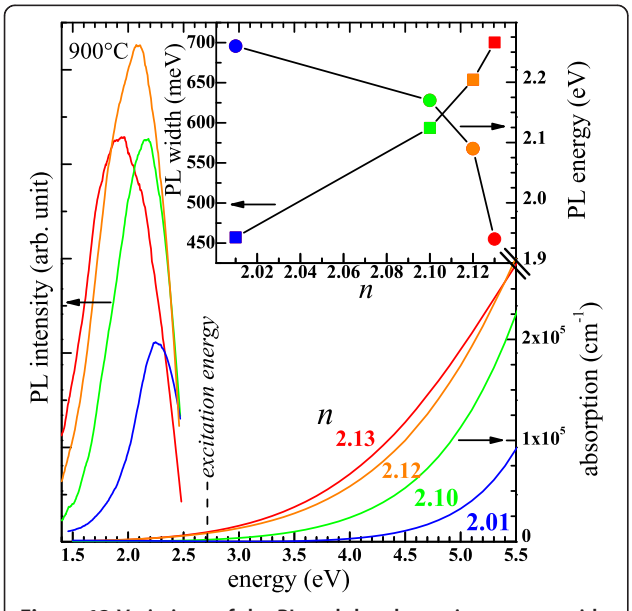

Figure 12 Variations of the PL and the absorption spectra with the refractive index *n*. The inset shows the evolution of the peak position and the band width with *n*.

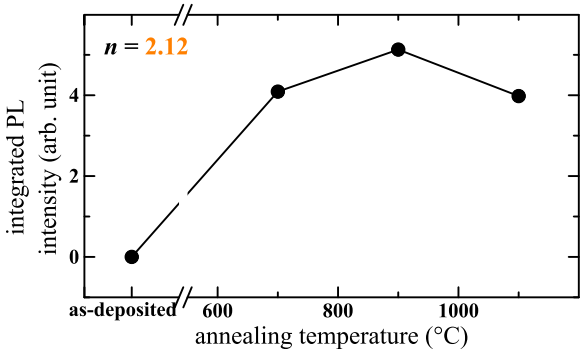

Figure 13 Evolution of the integrated PL intensity with the annealing temperature.

Laser annealing

Figure 14 shows the Raman spectra of one luminescent film with $n = 2.34$ recorded with various excitation power densities. Although we did not detect by Raman spectroscopy

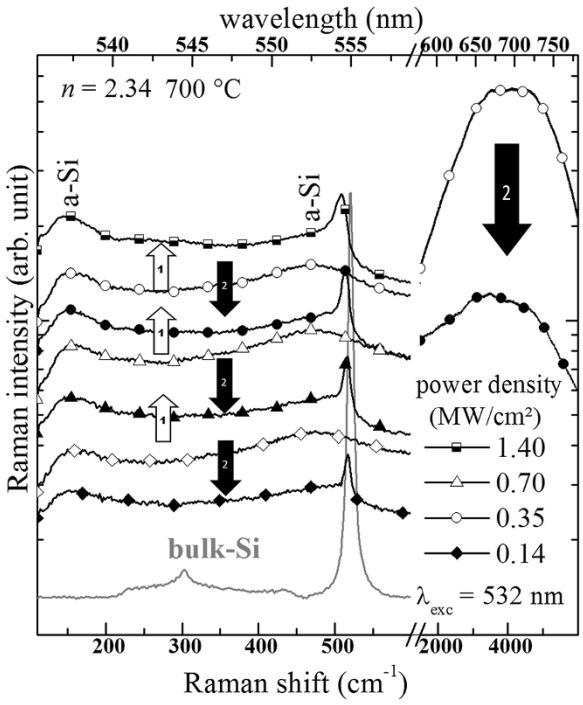

Figure 14 Laser annealing effect on the Raman spectra of SiN_x films deposited on fused silica substrates.

(Figure 7a) any crystalline Si-np even after annealing at 1100°C, we could however form small Si nanocrystals by laser annealing. This formation has been evidenced by Raman measurements that are separated in two steps for clarity. During the first step (white arrows), the power density of the laser was increased from 0.14 to 0.70 MW/cm^2. It is seen that the Raman signal increased because of the rise of the number of both Raman-scattered photons and PL photons. When the excitation power density reached 1.4 MW/cm^2, a sharp new Raman peak slightly shifted from that of bulk c-Si appeared. During the second step (black arrows), the power density was decreased back. One can observe that the c-Si peak remained whatever the power density suggesting that the structure of the SiN_x thin layer was definitively modified. This is then explained by the formation of small crystalline Si-np in the spot of the focused laser as observed elsewhere [45,50,51]. Moreover, one can notice that, for the same excitation densities, all baselines levels significantly dropped after the local formation of small Si nanocrystals. This drop of the baseline level is explained by the PL quenching of the broad PL band centered at about 700 nm, corresponding to approximately 4000 cm^{-1}, since the baseline is actually located on the green tail of the broad PL band. This demonstrates that this PL band cannot emanate from crystalline Si-np. This PL could however be related to amorphous Si-np. Nevertheless, Volodin et al. [45] showed that the presence of amorphous Si-np is not required for the laser-induced formation of crystalline Si-np which is in agreement with our results showing that this formation occurred in films containing a low Si content ($SiN_{0.9}$) and in as-deposited films as well.

Figure 15 shows the effect of the irradiation time on the Raman spectra of the latter SiN_x films during the laser annealing which was performed while the power density was set to 1.4 MW/cm^2 (Figure 14). The formation of small crystalline Si-np is very fast since the c-Si peaks at 300 and 510 cm^{-1} emerged almost immediately or at least in less than the acquisition time of approximately 0.5 s after the laser irradiation started. Moreover, one can observe that, after the laser-induced formation of crystalline Si-np, the Raman spectra changed while the thin SiN_x layer was continuously exposed to the intense radiation. Indeed, three modifications are clearly seen: (1) The baseline progressively dropped with increasing irradiation time which has been previously explained by the PL quenching of the material (see Figure 14). (2) The c-Si peak of 7.5 cm^{-1} shifted towards the position of c-Si in bulk material, and its intensity dropped after 1 min. However, its position and its intensity remained fixed for longer irradiation times. This latter modification, which is actually also discernible in Figure 14, can be explained by the unceasing growth of the crystalline Si-np until they reached a maximal size and/or by the relaxation of stress [46]. Also, (3) the intensity of the 2TA phonon mode at 300 cm^{-1} was quenched after 1 min of laser exposure which may result from disorder in the crystalline structure [52]. Besides, in the inset of Figure 15, a picture of the laser spot course while the thin layer was displaced perpendicularly to the laser beam is shown. This dark laser print reveals some local damages caused by the long exposition. However, since the main peak remains shifted to lower wavenumbers compared with bulk c-Si after a long illumination, one can assure that the film structure was definitively modified and that the films contained crystalline Si-np locally formed by laser annealing.

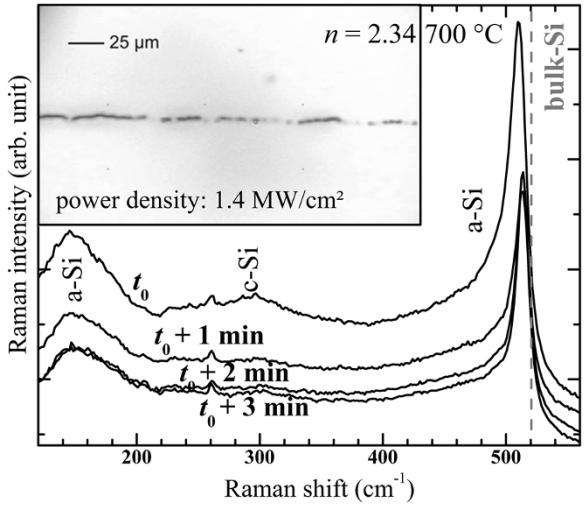

Figure 15 Effect of the irradiation duration on the Raman spectra of SiN_x films during the laser annealing. The inset shows the picture of the laser spot course on the SiN_x layer.

Discussion

The extensive investigation of the microstructure of SiN_x films versus the composition and the annealing treatments enables us to discuss on the PL origin considering that the films do not contain any oxygen and hydrogen. We show that neither defect states within the bandgap nor band tail states could account for all the aspects of the PL. Although we could form crystalline Si-np, we show that the radiative emission is not originating from confined states in crystalline Si-np but could be related to small amorphous Si-np.

Defect states in the bandgap

Optically active defect states within the bandgap of amorphous SiN_x could play a role in the radiative recombination of SiN_x as reported by several authors [18,53]. This interpretation is based on the wide PL spectra that contained distinct PL peaks with several energy levels that corresponded to the calculated values of various defect states found by Robertson [54,55]. Similar spectra were observed in the 1.75 to 3.1 eV spectral range by Ko

et al. [56] who noticed a redshift of the PL with decreasing Si content. This evolution is in contrast to that of our PL spectra which, moreover, do not contain any distinct PL peaks attributable to distinct defect state levels. As a consequence, we believe that the origin of the PL of our SiN_x samples cannot be ascribed to defect states localized within the bandgap.

Band tail recombination (static disorder model)

Let us consider the optical transition between photogenerated carriers localized in the band tail of the material in accordance with the static disorder model [57]. In this model, the carrier distribution in the exponential band tail density of states accounts for the PL band position and the PL shape of SiN_x:H [16]. An increase of the width of the localized states results in a blueshift and an increase of the width of the PL band. On one hand, many groups [13,16] explained that the increase of the structural disorder caused by the nitrogen alloying in Si-rich SiN_x:H with a very high Si content ($SiN_{x<0.6}$) accounts for the widening of the band tail states and then for the PL behavior. On the other hand, many groups [2-4] explained that the increase of the structural disorder induced by the incorporation of more nitrogen in N-rich $SiN_{x>1.33}$:H films accounts for the widening of the band tails and the PL properties. The increase of disorder in N-rich $SiN_{x>1.33}$ films with increasing N content is consistent with the FTIR spectra of Huang et al. [35] which show a drop of the LO band intensity.

Figure 5b showed that the situation is inversed in our Si-rich SiN_x films with a low Si excess content since the disorder manifestly increases with the Si incorporation. Therefore, the redshift of the PL band (Figure 12) cannot be explained by the tail-to-tail radiative recombination which would anyway be in contradiction with the widening of the PL band (inset of Figure 12). As a consequence, unlike Si-rich SiN_x:H films with a very high Si content ($SiN_{x<0.6}$) [13,16], we believe that the static disorder model cannot account for the PL properties of H-free Si-rich SiN_x films containing a low Si content ($SiN_{x>0.85}$). Besides, it has been shown that the hydrogen concentration plays an important role in the PL properties (intensity and peak position) of hydrogenated films [13].

Crystalline Si-np

Crystalline Si-np were detected by Raman, XRD, and HRTEM in numerous SiN_x films annealed at 1100°C that had a high $n > 2.5$ ($SiN_{x<0.8}$). Furthermore, we have demonstrated in Figure 8 that the progressive redshift of the crystalline Raman peak while n decreased is due to the decrease of the crystalline Si-np average size. The average sizes in the films with n ranging from 2.53 to 2.89 are between 2.5 and 6 nm, respectively. Theses sizes are theoretically small enough to show PL from excitons confined in crystalline Si-np according to the QCE model [58]. This model was proposed to explain the size dependence of the PL peak position that was noticed in oxide systems [1,59]. This size effect was evidenced in free crystalline Si-np surrounded by a thin Si oxide shell [60], which however slightly differ from that generally observed while the crystalline Si-np are embedded in a Si oxide host medium [59,61]. In the case of Si nitride as embedding matrix, several authors suggested that the PL could emanate from confined states in crystalline Si-np, which were present in the materials as attested by HRTEM observations, mainly because of a perceivable size effect on the PL [10-14]. Although our measurements (Figure 12) also show that the PL peak shifted to lower energies with increasing Si content, which is consistent with the QCE model, crystalline Si-np cannot be responsible for the radiative emission for two reasons: (1) Although small (2.5 to 6 nm) Si nanocrystals could be formed in films with $n > 2.5$ during annealing at 1100°C, we could not detect any PL. PL was detected only for smaller refractive indexes ($n < 2.4$). Besides, we demonstrated in Figure 7b and Figure 10 that this temperature is necessary to crystallize the excess of Si. Furthermore, (2) the PL of luminescent SiN_x films (*i.e.*, with $n < 2.4$) was quenched while we could form crystalline Si-np by another annealing method using an intense laser irradiation (Figure 14).

Amorphous Si-np

Although we have demonstrated that crystalline Si-np are not valid to explain the PL, let us consider Si-np with an amorphous phase as proposed by several authors [5-8]. The annealing temperature dependence of the FTIR spectra of one luminescent SiN_x film ($n = 2.22$) shown in Figure 6 suggests that a phase separation between Si-np and the Si nitride host media occurred during the annealing. The two Raman bands of a-Si at 150 and 485 cm^{-1} shown in Figure 7 indicate that luminescent films (*i.e.*, with $n < 2.4$) could contain amorphous Si-np. Besides, the Raman spectra would then show that the density of amorphous Si-np increased with increasing annealing temperature. This explains the absence of PL in the as-deposited samples and why the highest integrated PL intensity (Figure 13) was found at 900°C and not at 1100°C when crystalline Si-np could form. The redshift of the PL bands with increasing Si content (Figure 12) would then be due to a size effect. Also, the increase of the PL band width would then result from the widening of the size distribution as experimentally observed in Si oxide matrices [59,61]. Then, we have imaged a 1,000°C-annealed SiO_x/SiN_x multilayer by energy-filtered transmission electron microscopy enabling to distinguish small amorphous Si-np from the host media because of the high contrast of this technique. Because of PL interest, the refractive index of the SiN_x sublayer was set between 2.1 and 2.3. We could

distinctly observe amorphous Si-np in the 3.5-nm-thick SiO_x sublayers, but no particles were perceivable in the 5-nm-thick SiN_x sublayers [40]. Si-np could be however very small, below the EFTEM detection threshold of about 1 to 2 nm, and then constituted less than 1000 of Si atoms. Besides, such an amorphous Si-np size seems possible compared to the average size of 2.5 nm of crystalline Si-np detected by Raman spectroscopy in SiN_x with n = 2.53. Consequently, the origin of the PL would be related to small amorphous Si-np, and the recombination would originate either from confined states in the Si-np and/or from defect states at the interface between the Si-np and the Si nitride medium [7].

Conclusion

We have produced pure amorphous Si-rich $SiN_{x<1.33}$ thin films by magnetron sputtering with various Si contents using two deposition methods, namely the N_2-reactive sputtering of a Si target and the co-sputtering of Si and Si_3N_4 targets. The dependence of the only Si content on the microstructure and on the optical properties was studied. The two synthesis methods are equivalent since no systematic change could be discerned in the structural and the optical analyses. Besides, no trace of O atoms was detected by RBS and by FTIR, and no H bonded to Si or N could be detected by FTIR. We could then establish an empirical relation between the [N]/[Si] ratio and n based on the random bonding model on pure SiN_x which manifestly differs from previous relations that concerned SiN_x:H because of the H incorporation induced by the chemical deposition techniques.

Because of the absence of Si-H, N-H, and Si-O absorption bands, we could highlight the Berreman effect on the FTIR spectra of SiN_x by the normal incidence and an oblique illumination. The TO-LO pair modes of the two Si-N stretching absorption bands could be unambiguously assigned. A redshift of the two modes and a drop of the LO band intensity were observed while the Si content increased, which indicates that incorporation of more Si generates more disorder in the films. Moreover, a significant blueshift of the two modes with increasing annealing temperature was noticed which may be explained by a phase separation between Si-np and the Si nitride medium. At the same time, the LO band intensity increased indicating a rearrangement of the Si nitride network towards less disorder.

The effect of the annealing temperature on the Raman spectra has been investigated on films with n < 2.5 ($SiN_{x>0.9}$). The Raman spectra indicate that small amorphous Si-np could be formed during the annealing and that their density increased with the annealing temperature. For higher n (n > 2.5, $SiN_{x<0.8}$), Raman spectra, as well as XRD patterns, demonstrated that crystalline Si-np are formed upon annealing at 1100°C. Moreover, QCE on the optical phonon in crystalline Si-np embedded in Si nitride was observed. It matches with previous theoretical models concerning Si nanocrystals in Si oxide systems. The average size measured by HRTEM increased from 2.5 to 6 nm with increasing n.

Only SiN_x films with n ranging from 2.01 to 2.34 ($SiN_{x>0.9}$) exhibit visible PL. The PL bands redshifted and widened while n was increased. The tail to tail recombination cannot account for these PL properties since the FTIR spectra showed that the disorder increased with increasing n which would result in a blueshift and a widening of the PL bands. The PL could be then due to a QCE. The annealing temperature dependence of the PL intensity is consistent with the formation of Si-np. Nevertheless, the PL is not related to crystalline Si-np since they have not been detected in luminescent films by XRD and Raman measurements. As an additional proof, the PL quenched while Si crystalline Si-np could be formed by an intense laser irradiation. As a consequence, we believe that the PL is actually related to small amorphous Si-np and/or defect states that could be located at the interface between Si-np and the Si nitride host medium.

Competing interests

The authors declare that they have no competing interests.

Authors' contributions

OD wrote the article and carried the interpretation of the data. OD produced the samples and characterized them by spectroscopic ellipsometry, FTIR, absorption, PL, and Raman. JP carried out the RBS measurements. XP investigated the structure by HRTEM. SPN produced the multilayers. JC has been involved in the discussion about the origin of the PL. FG proposed and guided the project. All authors read and approved the final manuscript.

Acknowledgments

The authors acknowledge the French Agence Nationale de la Recherche, which supported this work through the Nanoscience and Nanotechnology Program (DAPHNÉS project ANR-08-NANO-005).

Author details

[1]CIMAP, UMR 6252 CNRS-ENSICAEN-CEA-UCBN, Ensicaen, 6 Bd Maréchal Juin, 14050 Caen, cedex 4, France. [2]UNIV PARIS 06, INSP NANOSCIENCE PARIS, CNRS, UMR 7588, 75015 Paris, France.

Received: 26 November 2012 Accepted: 29 December 2012
Published: 16 January 2013

References

1. Canham LT: **Silicon quantum wire array fabrication by electrochemical and chemical dissolution of wafers.** *Appl Phys Lett* 1990, **57:**1046.
2. Wang M, Xie M, Ferraioli L, Yuan Z, Li D, Yang D, Pavesi L: **Light emission properties and mechanism of low-temperature prepared amorphous SiN_x films. I. Room-temperature band tail states photoluminescence.** *J Appl Phys* 2008, **104:**083504.
3. Kistner J, Chen X, Weng Y, Strunk HP, Schubert MB, Werner JH: **Photoluminescence from silicon nitride—no quantum effect.** *J Appl Phys* 2011, **110:**023520.
4. Anutgan M, (Aliyeva) Anutgan T, Atilgan I, Katircioglu B: **Photoluminescence analyses of hydrogenated amorphous silicon nitride thin films.** *J Lum* 2011, **131:**1305.
5. Wang YQ, Wang YG, Cao L, Cao ZX: **High-efficiency visible photoluminescence from amorphous silicon nanoparticles embedded in silicon nitride.** *Appl Phys Lett* 2003, **83:**3474.

6. Park N-M, Kim T-S, Park S-J: **Band gap engineering of amorphous silicon quantum dots for light-emitting diodes.** *Appl Phys Lett* 2001, **78:**2575.
7. Dal Negro L, Yi JH, Kimerling LC, Hamel S, Williamson A, Gali G: **Light emission from silicon-rich nitride nanostructures.** *Appl Phys Lett* 2006, **88:**183103.
8. Rezgui B, Sibai A, Nychyporuk T, Lemiti M, Bremond G, Maestre D, Palais O: **Effect of total pressure on the formation and size evolution of silicon quantum dots in silicon nitride films.** *Appl Phys Lett* 2010, **96:**183105.
9. Nguyen PD, Kepaptsoglou DM, Ramasse QM, Olsen A: **Direct observation of quantum confinement of Si nanocrystals in Si-rich nitrides.** *Phys Rev B* 2012, **85:**085315.
10. Wang M, Li D, Yuan Z, Yang D, Que D: **Photoluminescence of Si-rich silicon nitride: defect-related states and silicon nanoclusters.** *Appl Phys Lett* 2007, **90:**131903.
11. Delachat F, Carrada M, Ferblantier G, Grob J-J, Slaoui A: **Properties of silicon nanoparticles embedded in SiNx deposited by microwave-PECVD.** *Nanotechnology* 2009, **20:**415608.
12. Kim T-Y, Park N-M, Kim K-H, Sung GY, Ok Y-W, Seong T-Y, Choi C-J: **Quantum confinement effect of silicon nanocrystals *in situ* grown in silicon nitride films.** *Appl Phys Lett* 2004, **85:**5355.
13. Molinari M, Rinnert H, Vergnat M: **Evolution with the annealing treatments of the photoluminescence mechanisms in *a*-SiN_x:H alloys prepared by reactive evaporation.** *J Appl Phys* 2007, **101:**123532.
14. Lelièvre J-F, De la Torre J, Kaminski A, Bremond G, Lemiti M, El Bouayadi R, Araujo D, Epicier T, Monna R, Pirot M, Ribeyron P-J, Jaussaud C: **Correlation of optical and photoluminescence properties in amorphous SiNx:H thin films deposited by PECVD or UVCVD.** *Thin Solid Films* 2006, **511–512:**103.
15. Yerci S, Li R, Kucheyev SO, van Buuren T, Basu SN, Dal Negro L: **Visible and 1.54 μm emission from amorphous silicon nitride films by reactive cosputtering.** *IEEE J Sel Top Quant* 2010, **16:**114.
16. Giorgis F, Mandracci P, Dal Negro L, Mazzoleni C, Pavesi L: **Optical absorption and luminescence properties of wide-band gap amorphous silicon based alloys.** *J Non-Cryst Solids* 2000, **588:**266–269.
17. Sahu BS, Delachat F, Slaoui A, Carrada M, Ferblantier G, Muller D: **Effect of annealing treatments on photoluminescence and charge storage mechanism in silicon-rich SiNx:H films.** *Nanoscale Res Lett* 2011, **6:**178.
18. Liu Y, Zhou Y, Shi W, Zhao L, Sun B, Ye T: **Study of photoluminescence spectra of Si-rich SiNx films.** *Matter. Lett.* 2004, **58:**2397.
19. Aydinli A, Serpengüzel A, Vardar D: **Visible photoluminescence from low temperature deposited hydrogenated amorphous silicon nitride.** *Solid State Comm* 1996, **98:**273.
20. Em Vamvakas V, Gardelis S: **FTIR characterization of light emitting Si-rich nitride films prepared by low pressure chemical vapor deposition.** *Surf Coat Tech* 2007, **201:**9359.
21. Mayer M: *SIMNRA User's Guide, Report IPP 9/113*. Garching: Max-Planck-Institut für Plasmaphysik; 1997.
22. Forouhi AR, Bloomer I: **Optical dispersion relations for amorphous semiconductors and amorphous dielectrics.** *Phys Rev B* 1986, **34:**7018.
23. HORIBA Scientific: http://www.horiba.com/scientific/products/ellipsometers/software/.
24. Bustarret E, Bensouda M, Habrard MC, Bruyère JC, Poulin S, Gujrathi SC: **Configurational statistics in a-$Si_xN_yH_z$ alloys: a quantitative bonding analysis.** *Phys Rev B* 1998, **38:**8171.
25. Hasegawa S, He L, Amano Y, Inokuma T: **Analysis of SiH and SiN vibrational absorption in amorphous SiN_x:H films in terms of a charge-transfer model.** *Phys Rev B* 1993, **48:**5315.
26. Lelièvre J-F, Fourmond E, Kaminski A, Palais O, Ballutaud D, Lemiti M: **Study of the composition of hydrogenated silicon nitride SiN_x:H for efficient surface and bulk passivation of silicon.** *Sol Energy Mater Sol Cells* 2009, **93:**1281.
27. Vernhes R, Zabeida O, Klemberg-Sapieha JE, Martinu L: **Pulsed radio frequency plasma deposition of a-SiN_x:H alloys: film properties, growth mechanism, and applications.** *J Appl Phys* 2006, **100:**063308.
28. Palik ED: *(Ed): Handbook of Optical Constants of Solids*. New York: Academic; 1985.
29. Guraya M, Ascolani H, Zampieri G, Cisneros JI, da Silva Dias JH, Cantão MP: **Bond densities and electronic structure of amorphous SiNx:H.** *Phys Rev B* 1993, **42:**5677.
30. Ono H, Ikarashi T, Ando K, Kitano T: **Infrared studies of transition layers at SiO2/Si interface.** *J Appl Phys* 1998, **84:**6064.
31. Lange P, Windbracke W: **Disorder in vitreous SiO_2: the effect of thermal annealing on structural properties.** *Thin Solid Films* 1989, **174:**159.
32. Lucovsky G, Yang J, Chao SS, Tyler JE, Czubatyj W: **Nitrogen-bonding environments in glow-discharge deposited *a*-Si:H films.** *Phys Rev B* 1983, **28:**3234.
33. Lin K-C, Lee S-C: **The structural and optical properties of *a*-SiN_x:H prepared by plasma--enhanced chemical-vapor deposition.** *J Appl Phys* 1992, **72:**5474.
34. Sénémaud C, Gheorghiu A, Amoura L, Etemadi R, Shirai H, Godet C, Fang M, Gujrathi S: **Local order and H-bonding in N-rich amorphous silicon nitride.** *J Non-Cryst Solids* 1997, **1073:**164–166.
35. Huang L, Hipps KW, Dickinson JT, Mazur U, Wang XD: **Structure and composition studies for silicon nitride thin films deposited by single ion bean sputter deposition.** *Thin Solid Films* 1997, **299:**104.
36. Dupont G, Caquineau H, Despax B, Berjoan R, Dollet A: **Structural properties of N-rich *a*-Si–N:H films with a low electron-trapping rate.** *J Phys D: Appl Phys* 1997, **30:**1064.
37. Batan A, Franquet A, Vereecken J, Reniers F: **Characterisation of the silicon nitride thin films deposited by plasma magnetron.** *Surf Interface Anal* 2008, **40:**754.
38. Berreman DW: **Infrared absorption at longitudinal optic frequency in cubic crystal films.** *Phys Rev B* 1963, **130:**2193.
39. Scardera G, Puzzer T, Conibeer G, Green MA: **Fourier transform infrared spectroscopy of annealed silicon-rich silicon nitride thin films.** *J Appl Phys* 2008, **104:**104310.
40. Pratibha Nalini R, Khomenkova L, Debieu O, Cardin J, Dufour C, Carrada M, Gourbilleau F: **SiO_x/SiN_y multilayers for photovoltaic and photonic applications.** *Nanoscale Res Lett* 2012, **7:**124.
41. Ippolito M, Meloni S: **Atomistic structure of amorphous silicon nitride from classical molecular dynamics simulations.** *Phys Rev B* 2011, **83:**165209.
42. Kirk CT: **Quantitative analysis of the effect of disorder-induced mode coupling on infrared absorption in silica.** *Phys Rev B* 1988, **38:**1255.
43. Xu X, Goodman DW: **Metal deposition onto oxides: an unusual low initial sticking probability for copper on SiO_2.** *Appl Phys Lett* 1992, **61:**774.
44. Tsu DV, Lucovsky G, Mantini MJ: **Local atomic structure in thin films of silicon nitride and silicon diimide produced by remote plasma-enhanced chemical-vapor deposition.** *Phys Rev B* 1986, **33:**706.
45. Volodin VA, Korchagina TT, Koch J, Chichkov BN: **Femtosecond laser induced formation of Si nanocrystals and amorphous Si clusters in silicon-rich nitride films.** *Physica E* 1820, **2010:**42.
46. Khriachtchev L, Räsänen M, Novikov S, Pavesi L: **Systematic correlation between Raman spectra, photoluminescence intensity, and absorption coefficient of silica layers containing Si nanocrystals.** *Appl Phys Lett* 2004, **85:**1511.
47. Richter H, Wang ZP, Ley L: **The one phonon Raman spectrum in microcrystalline silicon.** *Solid State Commun* 1981, **39:**625.
48. Paillard V, Puech P, Laguna MA, Carles R, Kohn B, Huisken F: **Improved one-phonon confinement model for an accurate size determination of silicon nanocrystals.** *J Appl Phys* 1921, **1999:**86.
49. Faraci G, Gibilisco S, Russo P, Pennisi AR: **Modified Raman confinement model for Si nanocrystals.** *Phys Rev B* 2006, **73:**033307.
50. Peng YC, Fu GS, Yu W, Li SQ, Wang YL: **Crystallization of amorphous Si films by pulsed laser annealing and their structural characteristics.** *Semincond Sci Technol* 2004, **19:**759.
51. Huang R, Wang DQ, Ding HL, Wang X, Chen KJ, Xu J, Guo YQ, Song J, Ma ZY: **Enhanced electroluminescence from SiN-based multilayer structure by laser crystallization of ultrathin amorphous Si-rich SiN layers.** *Opt Express* 2010, **18:**114.
52. Jain KP, Shukla AK, Abbi SC, Balkanski M: **Raman scattering in ultraheavily doped silicon.** *Phys Rev B* 1985, **32:**5464.
53. Deshpande SV, Gulari E, Brown SW, Rand SC: **Growth and photoluminescence of SiN_x thin films.** *J Appl Phys* 1995, **77:**6534.
54. Robertson J: **Electronic structure of silicon nitride.** *Philos Mag B* 1991, **63:**47.
55. Robertson J, Powell MJ: **Gap states in silicon nitride.** *Appl Phys Lett* 1984, **44:**415.
56. Ko C, Joo J, Han M, Park BY, Sok JH, Park K: **Annealing effects on the photoluminescence of amorphous silicon nitride films.** *J Korean Phys Soc* 2006, **48:**1277.
57. Boulitrop F, Dunstan DJ: **Phonon interactions in the tail states of a-Si:H.** *Phys Rev B* 1983, **28:**5923.

58. Proot JP, Delerue C, Allan G: **Electronic structure and optical properties of silicon crystallites: application to porous silicon.** *Appl Phys Lett* 1948, **1993:**61.
59. Takagi H, Ogawa H, Yamazaki Y, Ishizaki A, Nakagiri T: **Quantum size effects on photoluminescence in ultrafine Si particles.** *Appl Phys Lett* 1990, **56:**2379.
60. Ledoux G, Gong J, Huisken F, Guillois O, Reynaud C: **Photoluminescence of size-separated silicon nanocrystals: confirmation of quantum confinement.** *Appl Phys Lett* 2002, **80:**4834.
61. Garrido B, López M, Pérez-Rodríguez A, García C, Pellegrino P, Ferré R, Moreno J, Morante J, Bonafos C, Carrada M: **Optical and electrical properties of Si-nanocrystals ion beam synthesized in SiO_2.** *Nucl Instr and Meth in Phys Res B* 2004, **216:**213.

doi:10.1186/1556-276X-8-31
Cite this article as: Debieu *et al.*: Structural and optical characterization of pure Si-rich nitride thin films. *Nanoscale Research Letters* 2013 **8**:31.

Submit your manuscript to a SpringerOpen journal and benefit from:

► Convenient online submission
► Rigorous peer review
► Immediate publication on acceptance
► Open access: articles freely available online
► High visibility within the field
► Retaining the copyright to your article

Submit your next manuscript at ► springeropen.com